J. Fluid Mech. (1992), *vol.* 245, *pp.* 319–348

The late stages of transition to turbulence in channel flow

By N. D. SANDHAM† AND L. KLEISER
DLR, Institute for Theoretical Fluid Mechanics, Göttingen, Germany

(Received 23 September 1991 and in revised form 3 April 1992)

The late stages of transition, from the Λ-vortex stage up to turbulence, are investigated by postprocessing data from a direct numerical simulation of the complete K-type transition process in plane channel flow at a Reynolds number of 5000 (based on channel half-width and laminar centreline velocity). The deterministic roll-up of the high-shear layer that forms around the Λ-vortices is examined in detail. The new vortices arising from this process are visualized by plotting three-dimensional surfaces of constant pressure. Five vortices are observed, with one of these developing into a strong hairpin-shaped vortex. Interactions between the different vortices, and between the two channel halves, are found to be important. In the very last stage of transition second-generation shear layers are observed to form and roll up into new vortices. It is postulated that at this stage a sustainable mechanism of wall-bounded turbulence exists in an elementary form. The features which are locally present include high wall shear, sublayer streaks, ejections and sweeps. Large-scale energetic vortices are found to be an important part of the mechanism by which the turbulence spreads to other spanwise positions. The generality of the findings are discussed with reference to data from simulations of H-type and mixed-type transition.

1. Introduction

Transition from laminar to turbulent flow near a wall can proceed in a number of different ways, depending on the nature of the disturbances in the flow. The best understood process of transition is that beginning from very low levels of background noise. The mean flow, above a critical Reynolds number, is unstable to small-amplitude disturbances, and the process can be described well by linearized disturbance theory (the Orr–Sommerfeld equation). For incompressible two-dimensional mean flow, two-dimensional disturbances are the most rapidly amplified. Such waves (known as Tollmien–Schlichting or TS waves) remain two-dimensional during their nonlinear development and do not lead directly to turbulence. Further theoretical progress has been made by considering the linear instability of a modified base state, consisting of the basic laminar flow with superimposed finite-amplitude TS waves. This secondary instability theory (reviewed by Herbert 1988) was a major success of theoretical transition research in the 1980s. It explains the deformation of the TS waves into the experimentally observed Λ-shaped vortices. These Λ-vortices can be aligned in the streamwise direction (K-type transition), staggered (H-type),

† Present address: Department of Aeronautical Engineering, Queen Mary and Westfield College, Mile End Road, London E1 4NS, UK.

or a mixture of both. This is still far from turbulence, and it is the objective of this paper to examine some of the physical phenomena taking place in the later stages of transition.

Three key experimental investigations of transition in two-dimensional boundary layers appeared in the early 1960s and to a large extent motivated theoretical investigations of the transition process beyond the primary instability stage. All three generated two-dimensional disturbances artificially, and then followed the three-dimensional evolution of the flow. Much of the terminology for the late stages of transition comes from Klebanoff, Tidstrom & Sargent (1962). They described the breakdown process as an abrupt event, indicated by the appearance of spikes in the velocity–time traces. They associated these spikes with the formation of hairpin-shaped eddies in the high-shear layer that forms around the Λ-vortex. The idea that these eddies might form from an inflexional instability in the high-shear layer, amplifying high-frequency background disturbances, is what we now call the tertiary instability concept, which will be discussed later in this paper. The appearance of the spikes was associated with a kink in the high-shear layer by Kovasznay, Komoda & Vasudeva (1962), although they claimed that the spikes were not vortices. Hama & Nutant (1963) made detailed flow visualizations, which gave much insight into the details of the three-dimensional development of the flow. They observed the Λ-vortex develop into a vortex with an open tip, and then a breakdown into concentrated smaller-scale vortices. More detailed measurements of the Λ-vortex were made by Williams, Fasel & Hama (1984), resolving some earlier disagreements regarding the nature of the Λ-vortex and the high-shear layer around it.

A series of experiments in plane channel flow by Nishioka and co-workers have greatly added to our knowledge of the late stages of transition. Nishioka, Iida & Ichikawa (1975) demonstrated that essentially the same transition process takes place in channel flow as in boundary-layer flow, and confirmed theoretical predictions of a nonlinear subcritical instability. The concept of a tertiary instability, leading to hairpin vortices, was claimed to be confirmed by Nishioka, Asai & Iida (1980) (NB the terminology can be confusing – before the development of the secondary instability theory this instability was often called the secondary instability). Nishioka, Asai & Iida (1981) and Nishioka & Asai (1984) made detailed measurements of the flow field in the multi-spike stage. Connections were made to the flow features in fully developed turbulent flow, including streaks in the near-wall region. A review of the work of this group can be found in Nishioka (1985).

The work of Nishioka *et al.* (1980), claiming to confirm the presence of a tertiary instability, has been criticized by Kachanov *et al.* (1985) and Borodulin & Kachanov (1989). Kachanov *et al.* (1985) observed that the spike formation occurred strictly periodically and concluded that the formation of the spikes was a deterministic event, and therefore not a manifestation of a tertiary instability. Borodulin & Kachanov (1989) distinguished between the process of spike formation and the shear-layer instability. They claimed that the former is deterministic, while the latter leads to a 'randomization' of the flow. This conclusion has been supported by some numerical simulations by Rist (1990), who also made stability calculations similar to those of Nishioka *et al.* (1980).

Numerical simulation has emerged during the last decade as an additional tool for investigating the transition problem. The simulations are limited to simple geometries and low Reynolds numbers by the large computer resources that are required. However, they make possible the solution of simplified transition problems without empirical closure assumptions and have proved invaluable in establishing

the secondary-instability theory. A recent review of the techniques involved, and some of the successes of simulations, can be found in Kleiser & Zang (1991). An important feature of the simulations is that they provide access to three-dimensional fields of the pressure and all the components of velocity. These variables can also be accurately differentiated, which allows the study of quantities which cannot be accurately measured experimentally. A well-resolved simulation of the complete transition process in plane channel flow, using the temporal model (assuming periodicity in the streamwise direction), was made for the first time by Gilbert (1988).

The availability of complete flow-field information in a numerical simulation makes it worthwhile to re-examine the physical phenomena taking place in the late stages of transition. The intention of this paper is therefore to present a detailed account of the phenomenology of the later stages of transition, and to examine the mechanisms at work. A summary of the numerical database is given in §2, together with a discussion of the problem of vortex identification. In §3 we examine the roll-up into vortices of the high-shear layer that develops around the Λ-vortex, and describe in detail the space–time evolution of these vortices. An additional step in the transition process is presented in §4, this being the formation and roll-up of a second-generation shear layer and the appearance of an elementary form of wall-bounded turbulent flow. Further topics that are dealt with include the loss of predictability during the transition process (§5), the various large eddies that form during transition, together with the spanwise variation of properties such as skin friction (§6), and a discussion of the generality of the findings (§7).

2. Methodology

2.1. *Numerical simulation database*

Data for the current investigation are taken from a simulation by Gilbert (1988) of the transition process in plane channel flow with constant volume flow rate. The computational domain for the simulation is shown on figure 1. The streamwise direction is denoted by x_1, the spanwise direction by x_2, and the wall-normal direction by x_3. The lengths of the computational box are given by L_1, L_2 and L_3, and the velocity components by v_1, v_2 and v_3. All quantities are non-dimensionalized with the laminar centreline velocity and the channel half-width. Periodic boundary conditions are applied in x_1 and x_2, and zero-slip boundary conditions are applied on the walls.

The numerical method is fully spectral. The periodic directions are treated with Fourier expansions and the wall-normal direction with a Chebyshev expansion. The incompressibility constraint, including the no-slip boundary condition, is solved using the influence-matrix method of Kleiser & Schumannn (1980), a full description of which can be found in Canuto *et al.* (1988). The convective terms are de-aliased using the 3/2 rule. For all the data presented here the second-order Adams–Bashforth method was used for the time-advance of the nonlinear terms, together with Crank–Nicolson for the pressure and viscous terms. The simulation of K-type transition up to the multi-spike stage has been repeated with the Adams–Bashforth method replaced by a Runge–Kutta method of third-order accuracy, with no noticeable differences. All the simulations were run with an assumed spanwise symmetry about the plane $x_2 = \frac{1}{2}L_2$. This reduced the computer time and storage requirements by a factor of two. The same type of symmetry appears naturally in transition experiments, especially when periodic forcing in the spanwise direction is

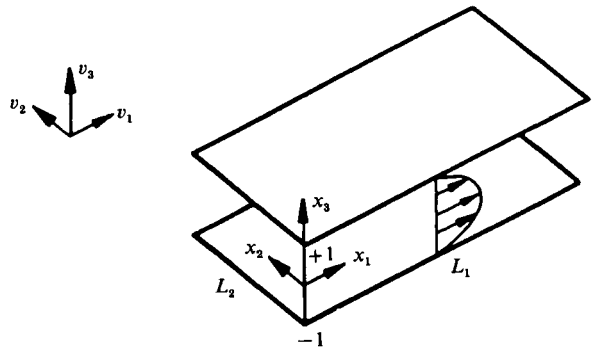

FIGURE 1. The computational domain. Subscript 1 refers to the streamwise direction, 2 to the spanwise direction, and 3 to the wall-normal direction.

applied (for example by sticking tape to the wall under the vibrating ribbon in the experiment by Klebanoff *et al.* 1962).

In this paper we will mainly present results from a simulation of K-type transition. Details of this simulation, together with an overview of the complete transition process up to statistically fully developed turbulence, can be found in Gilbert (1988) and Gilbert & Kleiser (1990). The Reynolds number was 5000, based on the channel half-width and laminar centreline velocity. The simulation began with a finite-amplitude (3% peak) TS wave, together with two equal and opposite oblique waves (amplitude 0.1%). For all these waves the eigenfunctions for v_1 and v_2 are antisymmetric in x_3, while the eigenfunction for v_3 is symmetric. Therefore there is a symmetry in the initial condition between the upper and lower channel halves – everything in the lower channel half is mirrored in the upper channel half, but shifted half a box length in the x_1 direction. The box lengths were $L_1 = 2\pi/1.12$, $L_2 = 2\pi/2.1$ and $L_3 = 2$. The reference frame for the simulation moves with the phase velocity c of the TS wave ($c = 0.28175$). Numerical resolution was raised during the simulation, as the energy content of higher modes increased, ending at 128^3 points. About eight orders of magnitude in kinetic energy were maintained between the largest and smallest wavenumbers all the way through the transition up to turbulence. Resolution requirements are largest in the late stages of transition, and the final turbulent state is probably a little over-resolved. Gilbert (1988) found that statistics from the fully developed turbulent state were in good agreement with the simulations of Kim, Moin & Moser (1987).

Several other transition cases have been investigated using the same code. N. Gilbert (1989, unpublished) has simulated a case of mixed transition, where several two- and three-dimensional waves, each consisting of many Orr–Sommerfeld modes, were used for the initial condition. The box for this simulation was twice as large in x_1 and x_2, and a peak resolution of $N_1 \times N_2 \times N_3 = 160 \times 160 \times 128$ was used. Härtel & Kleiser (1992) have simulated the pure subharmonic case, similarly on a $160 \times 160 \times 128$ grid. The computational box in this case was twice that of the K-type simulation in the streamwise direction, and the same in the spanwise direction. In the current work these other databases have been used to check the generality of our findings. Detailed results will not be presented here, but comments will be made as appropriate. All the simulations have been made for a Reynolds number of 5000.

Some comment on the temporal nature of the simulation is in order. In a direct numerical simulation one selects appropriate initial and boundary conditions and

then solves the governing equations of motion. Then, assuming that adequate resolution is made in space and time, one has a complete solution to the given problem. Such solutions of the Navier– Stokes equations are of much interest in their own right, since the available analytic solutions are rather meagre. A separate question to be asked is how well the temporal model problem translates to the laboratory flow, where there is no periodicity in the streamwise direction. In the temporal channel flow the solutions to the Navier–Stokes equations exhibit laminar flow, linear instability, secondary instability, Λ-vortices, high-shear-layer breakdown and turbulence in the temporal simulation just as in the experiments. Statistics for the turbulent flow are in good agreement with recent experiment results (Nishino & Kasagi 1989). Thus there is good reason to believe that physical phenomena which occur on a length-scale smaller than the computational box length (almost certainly everything that happens beyond the Λ-vortex stage) are captured in the temporal simulations. One must always be on the look-out for phenomena which might be different in the spatial and temporal approaches. However, in this investigation we have found no evidence for any such deviation. Further discussion on this point is provided in Kleiser & Zang (1991, §3.4).

2.2. *Vortex identification*

A vortex is an entity that is conceptually very easy to appreciate, but which is difficult to formulate precisely. In the current application we have vortex motions in a three-dimensional space, evolving rapidly in time. In order to make full use of the enormous amount of data from the simulations, it would be useful to have a scalar measure of a vortex, whose size gave the strength of the vortex. Such a measure could then be used to follow the vortices as they evolve in space and time using computer graphics. Unfortunately no perfect measure of a vortex is known. Vorticity is problematic, since it canot distinguish between shear layers and vortices – any shear layer has vorticity, whether or not vortices are present. In the problem under consideration this failure has already led to confusion over whether the kinks that form in the high-shear layer around the Λ-vortices are really vortices (Kovasznay *et al.* 1962). Also vortex lines (lines everywhere parallel to the local vorticity vector) are inadequate. Kleiser & Laurien (1985) showed that the Λ-vortex does not necessarily consist of a bunch of vortex lines. Conversely, Robinson (1991) demonstrated that vortex lines can given the illusion of hairpin vortices, even when there are no such vortices in a flow.

An alternative measure of a vortex has been developed by considering expansions around critical points in a flow field (see Perry & Chong 1987 for a review). The local topology of the flow can be found by examining the eigenvalues of the velocity-gradient tensor $\partial v_i/\partial x_j$. Hunt, Wray & Moin (1988) have advocated the second invariant of the velocity gradient tensor as a scalar measure to locate vortices in space. In their notation

$$\mathrm{II} = \frac{\partial v_i}{\partial x_j}\frac{\partial v_j}{\partial x_i}, \tag{1}$$

which for incompressible flows is equal to $-2Q$ in the notation in Chong, Perry & Cantwell (1990). Large negative values of II indicate regions in the flow where vorticity dominates over strain.

Another measure of a vortex is the static pressure. Static pressure is a relative minimum in the centre of a region of strong rotational fluid motion, and the size of the pressure depression gives a measure of the strength of a vortex. Although this

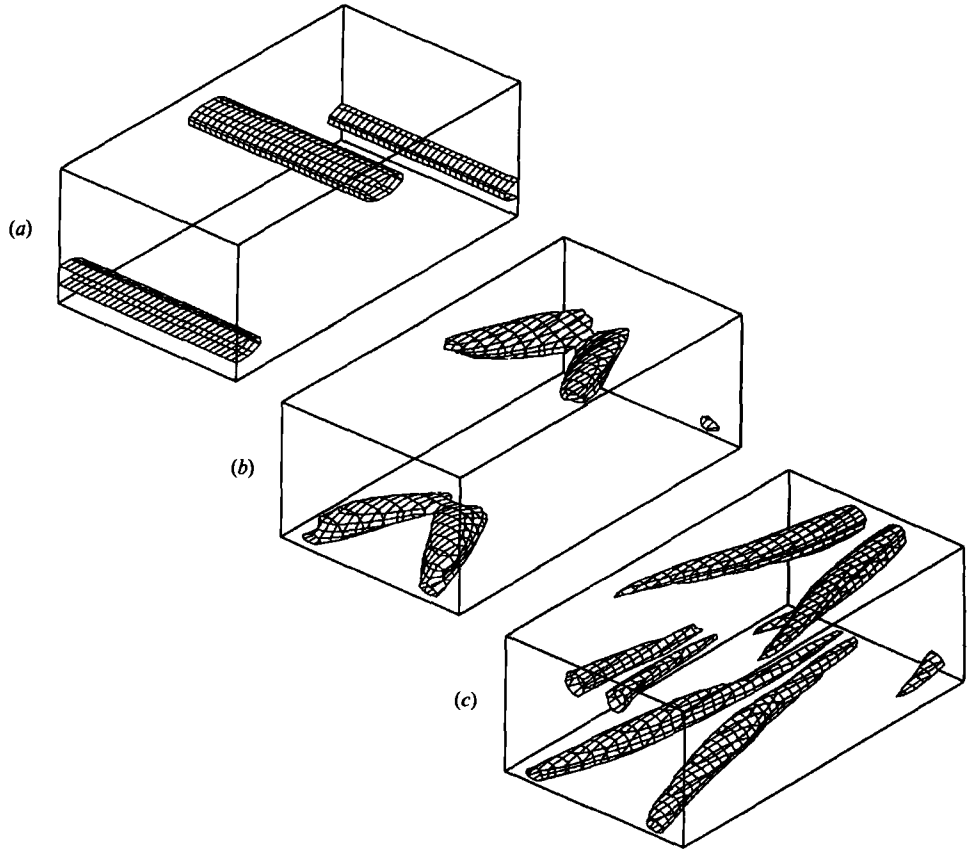

FIGURE 2. Three-dimensional views of a surface of constant II (the second invariant of the velocity-gradient tensor): (a) $t = 0$, II $= -0.025$, showing the initial condition of two vortices corresponding to an antisymmetric TS wave; (b) $t = 100$, II $= -0.03$, showing the Λ-vortex which forms from the secondary instability; (c) $t = 124$, II $= -0.04$, showing the open-tip Λ-vortices.

seems rather obvious pressure has rarely been used to locate vortices, since it is difficult to measure experimentally. It is not guaranteed that every pressure minimum is a vortex, and one really needs a confirming plot of the local velocity vectors in a plane perpendicular to the axis of the vortex, and in a reference frame moving with the vortex, to be certain that a vortex exists. Pressure proved to be a useful diagnostic in a study of the compressible mixing layer by Sandham & Reynolds (1991), where a close correspondence was found between the structure of the pressure field and the transport of a passive scalar.

Both the second invariant II and the static pressure p' (relative to the mean wall pressure) have been used in the current work. The conclusion is that the different measures of a vortex are useful at different stages of the transition process. In the early stages, where the vortices are relatively weak, II appears to be a good measure. Figure 2 shows the computational box together with a surface of constant II, whose level was chosen to be close to the negative maximum. The sequence shows the evolution from a two-dimensional finite-amplitude TS wave at time $t = 0$ in the simulation, through the Λ-vortex stage at $t = 100$, and eventually leading to an open-tip Λ-vortex, as observed by Hama & Nutant (1963). Similar results were obtained by H. Vollmers (1984, unpublished) using data from Kleiser

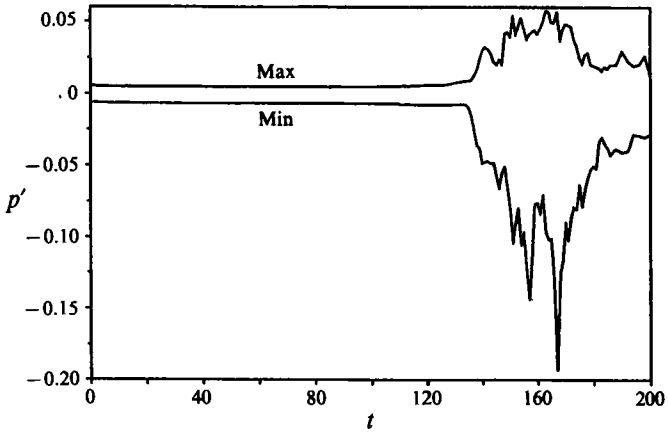

FIGURE 3. The maximum and minimum of pressure p' (relative to the mean wall pressure) in the flow field as a function of time. Note the sharp change at $t = 134$, the strong variations during transition, and the calming of the flow for $t > 180$ as a mature turbulent state is approached.

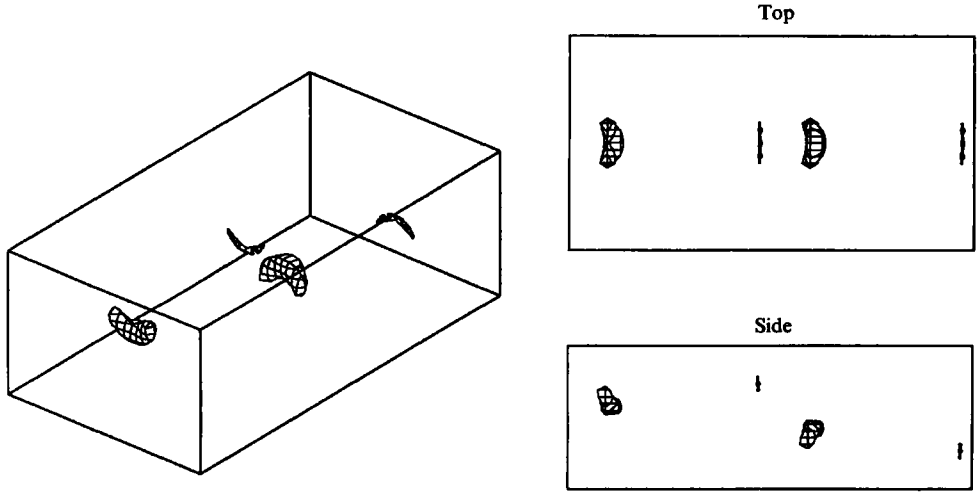

FIGURE 4. Three views of the surface of pressure $p' = -0.014$ at $t = 138$.

(1982) and plotting the discriminant of the velocity-gradient tensor (Vollmers, Kreplin & Meier 1983). The symmetry between the upper and lower channel halves (see §2.1) and the periodicity in x_1 and x_2 should be noted in all our figures. As new vortices began to appear in the flow the utility of II diminished, since the flow pictures became too complicated. A better measure for locating the new vortices turned out to be the pressure. A plot of the minimum and maximum of p' in the flow field as a function of t is shown on figure 3. It can be seen that a dramatic change takes place at around $t = 134$, when strong vortices emerge from the shear layer. This point appears to be very well defined and could perhaps be used to define the onset of breakdown precisely. These new vortices have a very prominent pressure depression in their cores. A visualization in three dimensions is shown on figure 4 at $t = 138$, together with top and side views. A detailed description of these vortices is postponed until the next section. In this paper we are interested in the later stages of transition, and the pressure has proved to be the most useful scalar quantity to

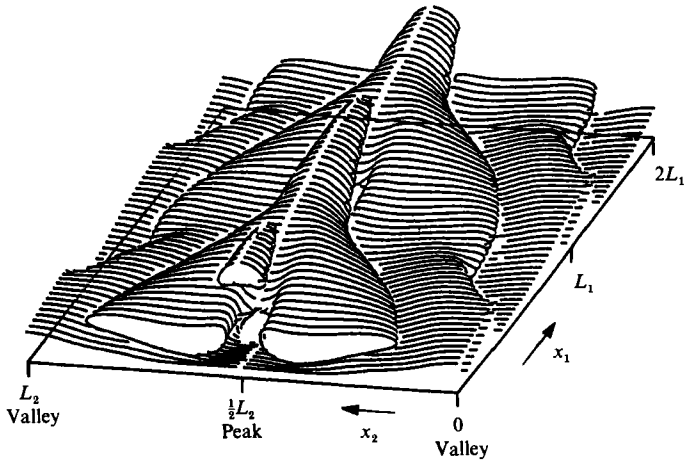

FIGURE 5. View of the high-shear layer ($\partial v_1/\partial x_3 = 1.65$) at $t = 128$ from Gilbert (1988). Note that two periods are plotted in the streamwise direction.

locate vortices. In important cases, as pointed out in the text, we have used II and velocity vectors, to ensure some redundancy in the identification of a vortex.

3. High-shear-layer roll-up and vortex evolution

The Λ-vortex, which develops from the secondary instability in plane channel flow, generates a shear layer. The mechanism for the formation of this shear layer is vortex stretching and convection, as demonstrated in a simpler flow by Stuart (1965, 1984). A view of this shear layer, located by an iso-surface of high $\partial v_1/\partial x_3$ is shown on figure 5 (from Gilbert 1988). Fluid that is ahead and to the sides of the Λ-votex is forced down towards the wall, resulting in high shear at the wall. Behind the Λ-vortex, fluid is moved away from the wall and vortex stretching results in a region of high shear that is detached from the wall. It is this region of high shear, situated near the plane of symmetry $x_2 = \frac{1}{2}L_2$, that first becomes important. This plane of symmetry is known as the 'peak' plane, since the velocity fluctuations, measured over one TS cycle, are largest here compared to other spanwise locations. The other plane of symmetry at $x_2 = 0$ is known as the 'valley' plane.

The high-shear layer at the peak plane develops a kink at around time $t = 136$ in the simulation. This can be seen on figure 6(a), which shows a cut through the shear layer at the peak plane in the lower half of the channel for times $t = 134$ to 146. Contours of shear $\partial v_1/\partial x_3$ equal to 2, 4 and 6 are shown. The first kink in the shear layer occurs at $t = 136$ ($x_1 = 2.4$, $x_3 = -0.2$). This can be compared with the first spike stage in Kovasznay *et al.* (1962). The kink in the shear layer moves to the right as time proceeds, indicating that it is moving at a velocity higher than the phase speed of the TS wave, with which the computational domain moves. The velocity of the kink is approximately 75% of the laminar centreline velocity.

The kink in the high-shear layer indicates the roll-up of a vortex. Figure 6(b) shows pressure contours for the same times as in figure 6(a). The pressure is plotted in intervals of 0.005, with negative values (low-pressure regions) shown with dashed contours. The vortex that is responsible for the kink in the shear layer shows up as a region of low pressure, with locally circular pressure contours, at $t = 136$ ($x_1 = 2.5$, $x_3 = -0.2$). The same regions showed up as negative minima in II from equation (1),

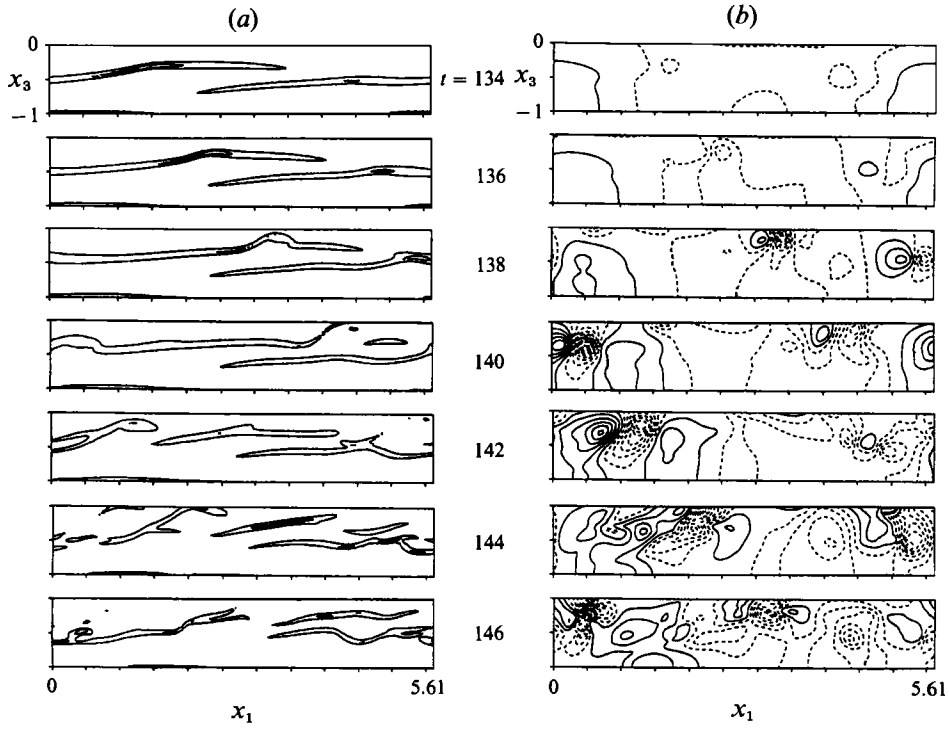

FIGURE 6. Cuts through the peak plane for times $t = 134$ to 146: (*a*) shear ($\partial v_1/\partial x_3 = 2$, 4 and 6); (*b*) pressure p' (contour spacing 0.005, negative contours dashed).

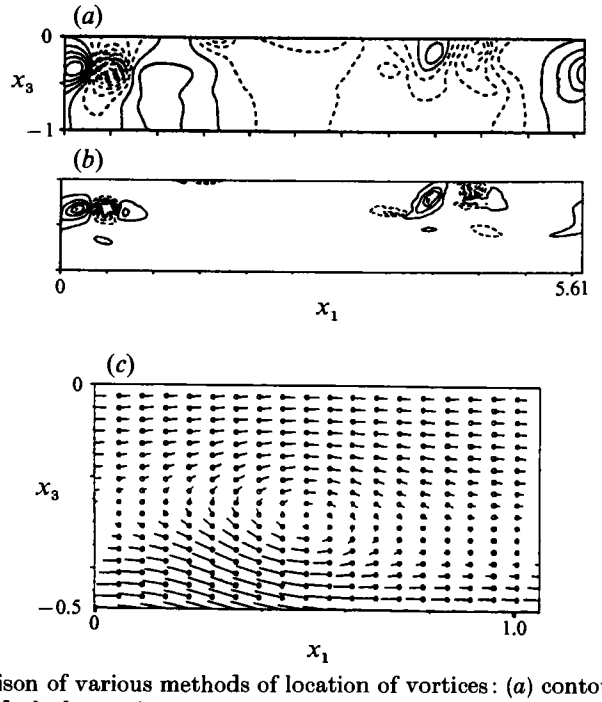

FIGURE 7. Comparison of various methods of location of vortices: (*a*) contours of p', (*b*) contours of II (in each case dashed negative contours correspond to vortices) and (*c*) local velocity vectors for the vortex near $x_1 = 0.5$, $x_3 = -0.3$.

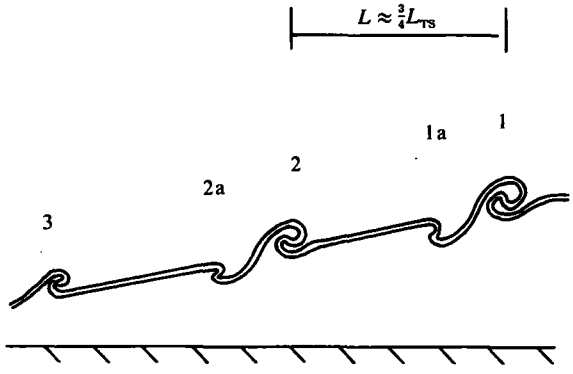

FIGURE 8. Sketch of the shear-layer roll-up process, showing the observed levels of roll-up.

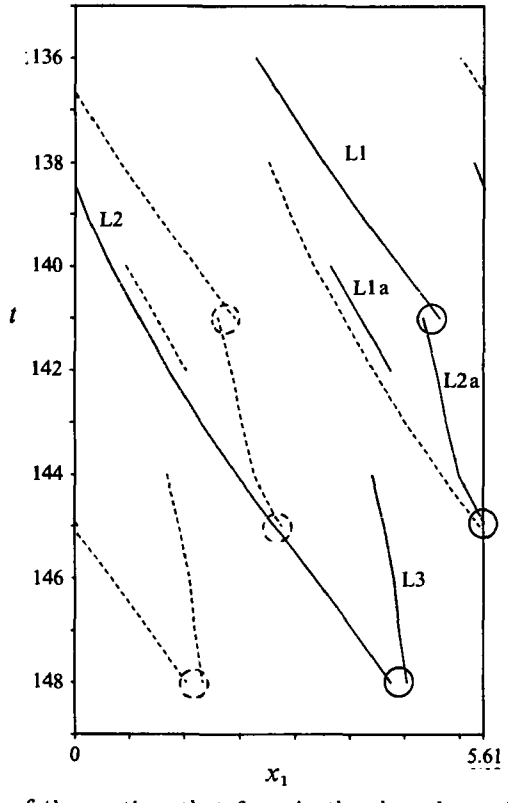

FIGURE 9. Trajectories of the vortices that form in the shear layer, located by the minima of pressure at the peak plane: ——, lower; – – –, upper channel half. The reference frame is chosen so that the TS wave is stationary. The circles show the locations of vortex interactions.

and also as locally circular instantaneous streamlines, when a reference frame moving with the pressure minimum was chosen. Thus, the kinks in the shear layer are definitely associated with the roll-up of vortices. A direct comparison of the various measures of identifying a vortex is made on figure 7 at the slightly later time of $t = 140$. Figure 7 (*a*) shows p' contours, figure 7 (*b*) contours of II, and figure 7 (*c*) velocity vectors for the vortex near $x_1 = 0.5$, $x_3 = -0.3$ (using a reference velocity of 0.8). All the measures agree on the location of vortices in the flow.

A total of five vortices develop in the shear layer in each channel half, and appear as local pressure minima on figure 6(*b*). A simplified picture of the shear-layer roll-up is sketched on figure 8. The roll-up produces pairs of vortices, although the second vortex in each pair can be so weak as to be insignificant. The pairs of vortices are separated from each other by a fairly large distance (very roughly $\frac{3}{4}$ of a TS wavelength). We will refer to the vortices by the channel half in which they originate (L = lower, U = upper), the number of the roll-up (1, 2 or 3), and an additional 'a' for the second vortex of each pair. From the first level of roll-up we have the vortex L1, which develops at $t = 136$ ($x_1 = 2.5$, $x_3 = -0.2$ on figure 6), and L1a, which can be seen at $t = 140$ ($x_1 = 3.5$, $x_3 = -0.3$). The second level of roll-up produces L2 at $t = 138$ ($x_1 = 5.5$, $x_3 = -0.35$) and L2a at $t = 142$ ($x_1 = 5.0$, $x_3 = -0.5$). The third and last level of roll-up produces L3 at $t = 144$ ($x_1 = 4.1$, $x_3 = -0.5$). The vortex L3 rolls up the fluid at the end of the original shear layer and is the last vortex to develop out of the shear layer. Vortices L1, L2, L2a and L3 are strong enough to produce a significant local drop in pressure.

The movement of the various vortices is shown on an x_1–t plot on figure 9. The vortices are located by their pressure minima in the peak plane. Vortices in the lower half of the channel are marked with solid lines, while vortices in the upper channel half are shown dashed. Interactions between the vortices are marked with circles and will be discussed later. On the plot a trajectory at 45° would be a vortex moving at the laminar centreline velocity, while a vertical line would be a vortex moving with the velocity of the TS wave. It can be seen how the vortices L2 and U2 speed up with time, indicating that the cores of the vortices move towards the centre of the channel. Vortices developing later in the simulation tend to be moving more slowly than the earlier vortices since they originate in the portion of the high-shear layer closer to the wall.

The time of each vortex formation can be quantified by finding the time when the pressure drops 0.025 below the mean wall pressure. Thus computed, these vortices form at $t = 136$, 139, 143 and 146. The times compare well with the times for the spike stages 2 to 5, found by Gilbert (1988) to be at $t = 136$, 140, 144 and 148. Gilbert's first spike stage appears to be associated with the formation of the high-shear layer at around $t = 128$. It should be noted that the definition of a spike is a rather subjective matter. The vortices that show up in the pressure contours are small compared to the TS wavelength, and relatively energetic since the pressure depression is much stronger than for the original Λ-vortex. These vortices will clearly show up as spikes in the velocity signal measured by a probe in the flow (cf. figure 22 in Gilbert 1988).

The mechanism for *growth* of the vortices once they have formed is evidently that of a shear-layer instability, with energy being extracted from the local mean flow into the vortex. However, there are significant differences between the vortex *formation* and a Kelvin–Helmholtz instability wave. If the vortices were to develop from an instability wave in a uniform shear layer, triggered by background noise, one would expect them to be approximately uniformly spaced along the shear layer, and not to occur at the widely spaced intervals actually observed. Of course, the shear layer encountered in the simulation is not uniform and is inclined relative to the flow direction. We discuss the vortex formation process further in §7.2.

The three-dimensional evolution of the shear-layer vortices is next considered, using a surface of constant pressure to locate the cores of the vortices in space. On figure 4 oblique, side and top views of the surface $p' = -0.014$ at $t = 138$ were shown. When viewing these plots one should bear in mind the periodicity of the flow in x_1

and x_2. The staggered symmetry between the upper and lower channel halves was explained in §2.1. The first two levels of roll-up (vortices L1, L2, U1 and U2) are visible and can be compared with the cuts through the peak plane in the lower channel half (figure 6*b*). At this time in the simulation all the vortices have a banana shape, centred on the peak plane with the ends pointed towards the wall.

The vortical structures which originate from the shear-layer roll-up dominate the flow up to time $t = 148$. A sequence from $t = 141$ to 148 is shown on figure 10, for the pressure surface $p' = -0.025$. The first vortices L1 and U1 remain weak, and do not show up at this (lower) pressure level. From $t = 141$ to 147 the vortices L2 and U2 develop legs and have the appearance of hairpin vortices. The vortices L2a and U2a appear first as barrel-shaped vortices ($t = 144$). They then interact with the hairpin vortices in the other side of the channel (L2*a* interacts with U2, U2a interacts with L2). This interaction can be classified as a *cross-channel interaction* and was marked on figure 9 with a circle at $t = 143$. Such interactions have been observed in simulations by Zang & Krist (1989). They found them to be Reynolds-number dependent, and less important at higher Reynolds numbers. The head of the hairpin wins out in this interaction and all that is left of the 2a vortices are the 'streamers' behind the hairpin vortices, visible at $t = 146$. The third and last level of roll-up appears as barrel-shaped vortices (L3 and U3) at $t = 147$, which interact with the hairpins at $t = 148$ (L2–L3 and U2–U3). This interaction can be classified as an *overtaking interaction*, since the second level of roll-up interacts with the third level of roll-up from the next shear layer to the right. Such interactions have been observed in the experiments (see Klebanoff *et al.* 1962), and do not appear to be affected by the temporal nature of the simulation. The location of this interaction is marked at $t = 148$ on figure 9. The main hairpin vortices L2 and U2 were also observed in surfaces of II. A qualitative difference was that the legs were longer with this measure. Vortices L1 and U1 had a hairpin shape when measured with II, but only the heads developed a pressure minimum. The other vortices did not appear as hairpins, either in p or II.

In isolation a hairpin vortex will develop into a vortex ring, as shown in a vortex-filament computation by Moin, Leonard & Kim (1986). In their computations a hairpin vortex was found to pinch off, leaving behind a vortex ring. This pinching process appears to be taking place in the present numerical simulation and is visible at $t = 147$ near the tip of the hairpin. However, at about this time the hairpin interacts with the third level of roll-up and, since the head of the hairpin and this roll-up are rotating in the same direction, joining into a vortex ring is not possible. Thus, the evolution of a hairpin vortex into a vortex ring is sensitive to other events in the flow.

Many of our observations from the simulations are similar to observations made by Hama & Nutant (1963) in boundary-layer transition, although we must explain some of the differences in nomenclature. What they refer to as a vortex loop is our Λ-vortex. It originates as a warping of the TS wave, and eventually develops into an open-tip Λ-vortex (see figure 2). Hama & Nutant also observed a breakup of the high-shear layer into concentrated vortices. What they refer to as a secondary Λ-vortex, and later as an Ω-vortex is probably our hairpin vortex L2. The tangling which they observed at the neck of this vortex could be the effect of the hairpin vortex developing towards a vortex ring. They refer to this tangle of vortices as the appearance of turbulence. Their 'tertiary' vortices are probably the other vortices that develop from the shear layer, for example L3. Thus to a large extent the observations of Hama & Nutant appear to be compatible with the current analysis

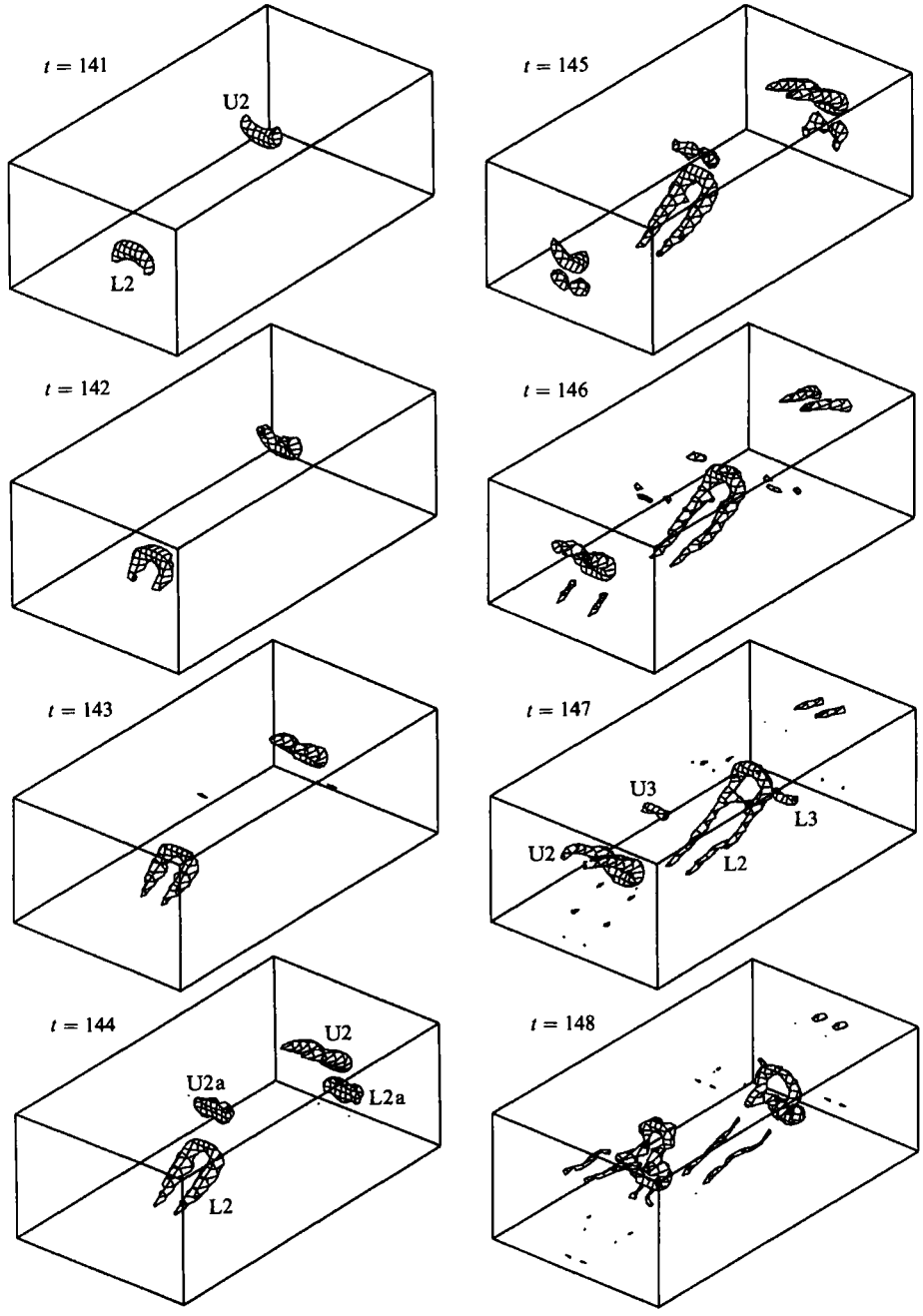

FIGURE 10. A time sequence of the pressure surface $p' = -0.025$ showing the three-dimensional evolution of the vortices that originate in the high-shear layer. Vortices L2 and U2 develop into pronounced hairpin vortices.

and suggest a very close correspondence between boundary-layer and channel flow transition.

The breakup of the hairpin vortex and the interaction with the third and last level of roll-up marks the end of this phase of the transition process. We are left at $t = 150$ with the structure shown on figure 11. The interior of the channel is a complicated

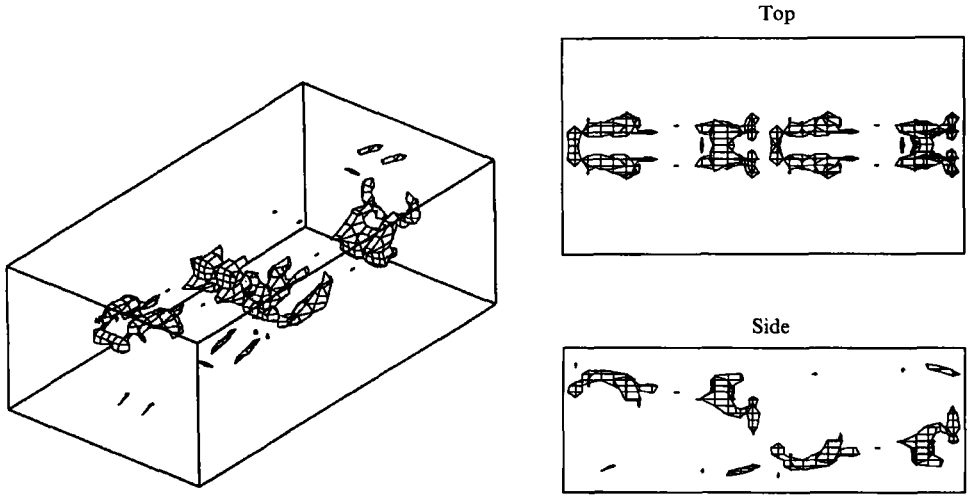

FIGURE 11. Three views of the surface of pressure $p' = -0.025$ at $t = 150$ after the breakup of the hairpin vortex.

tangle of vortices. However, the top view shows that this is still confined to a small region around the peak plane where the original roll-up took place. Also the skin friction and the centreline velocity are still close to their laminar values (see later). Thus we still have not arrived at a turbulent flow.

4. Elementary wall turbulence

In order to determine whether transition to turbulence is complete, one must decide what is meant by turbulence. In this section the development of the mechanics of *near-wall* turbulence will be examined. Detailed experimental observations of this phenomenon, which is characterized by high wall shear, sublayer streaks, ejections and sweeps, began with the work of Kline *et al.* (1967). A review of the current level of understanding can be found in Robinson (1991). Earlier work on this theme, using the present simulation database, can be found in Gilbert (1988) and Gilbert & Kleiser (1990).

A new shear layer forms at the peak plane by $t = 151$. This is shown on figure 12 by contours of shear (levels 2, 4 and 6 as before) and pressure (intervals of 0.01), together with times $t = 153$ and 155. The new shear layer is located in the first half of the channel $0 < x_1 < \frac{1}{2}L_1$ at approximately $x_3 = -0.7$. We will refer to this shear layer as a second-generation shear layer. It is rather narrow in the spanwise direction (maximum width $\frac{1}{6}L_2$) and appears to form by the same mechanism of vortex stretching and convection (Stuart 1965) that led to the shear layer around the Λ-vortex. A sketch of the location of the shear layer is shown on figure 13. The vortices that cause the shear layer are nearly streamwise vortex pairs in the near-wall region that arise from the previous events in the flow. In the current stimulation there are three such pairs of vortices. One pair arises from the remnants of the hairpin legs, another from the remnants of the cross-channel interaction, and a third from the L1 vortex that was weak and inconsequential in the earlier stages of transition. The last pair of vortices appears to play the strongest role in generating the second-generation shear layer shown on figure 12. These vortices can be seen on figure 11 near the lower wall at $x_1/L_1 = 0.42$ and near the upper wall at $x_1/L_1 = 0.92$.

As well as creating the detached secondary shear layers, such streamwise

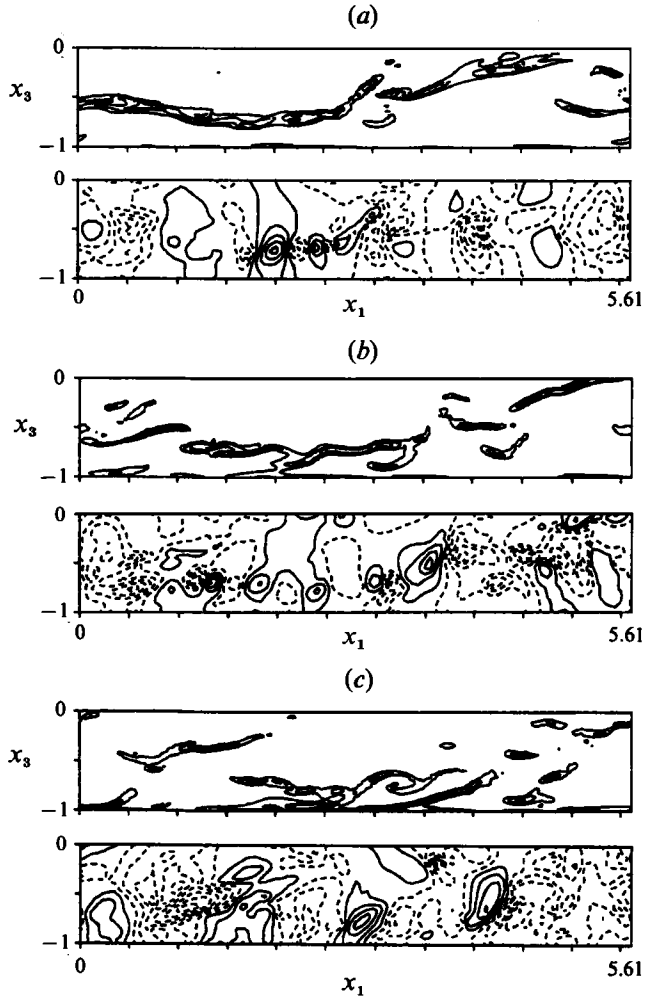

FIGURE 12. The formation and roll-up of a second-generation shear layer: (*a*) $t = 151$, (*b*) 153 and (*c*) 155. In each case the upper plot shows shear (contour levels $\partial v_1/\partial x_3 = 2$, 4, and 6) and the lower plot pressure (contour spacing 0.01) in the peak plane.

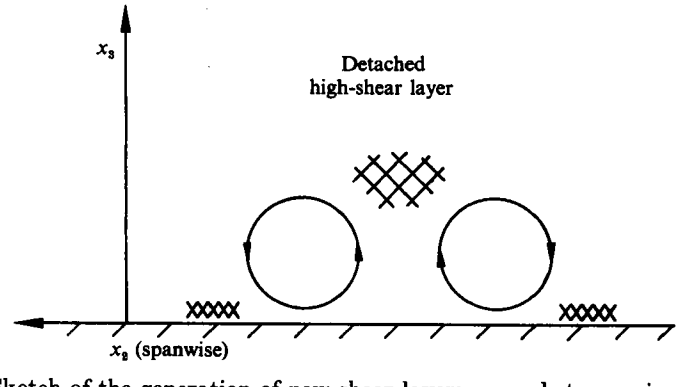

FIGURE 13. Sketch of the generation of new shear layers around streamwise vortices by a process of vortex stretching and convection (after Stuart 1965).

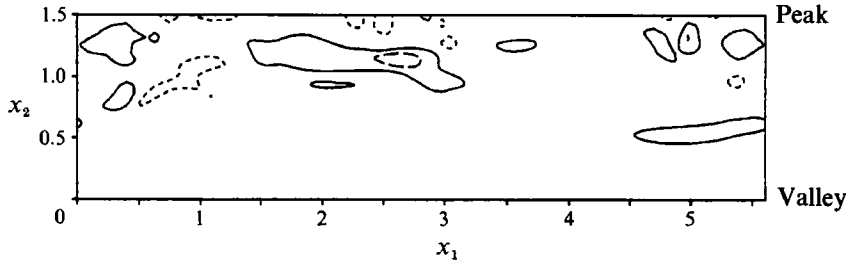

FIGURE 14. Wall shear at $t = 155$, showing the first regions of high wall shear. Contours are shown of $\partial v_1/\partial x_3 = 0$ (- - - - -), 10 (——) and 20 (– – – –).

vortices act to generate high wall shear (see figure 13) on the opposite side of the vortex to the detached shear layer. Figure 14 shows the shear $\partial v_1/\partial x_3$ at the wall at $t = 155$. For the first time in the simulation there are regions of high wall shear. These regions form at a distance of $\frac{1}{8}L_2$ from the peak plane, whereas the original vortices that caused them were located at approximately $\frac{1}{12}L_2$. There is a time delay of approximately 4 time units between the appearance of the vortices and the generation of high wall shear. This allows for convection towards the wall to take place. The region between the two areas of high wall shear, either side of the symmetry plane $x_2 = \frac{1}{2}L_2$, is the first low-speed streak in the simulation. The wall shear at $t = 155$ can be compared with the plot of the sublayer velocity from Nishioka & Asai (1984). The same general pattern of the two short regions of high-speed fluid around a low-speed streak can be seen. One apparent difference between simulation and experiment is the observation in this experiment of a region of high shear on the wall at the nominal peak plane. Such a region is not observed in the simulations. The explanation lies in the fact that in the experiment there was no spanwise forcing. Thus the streaks that form are not exactly symmetric about the peak plane, and it appears that the peak plane chosen in the experiments cuts slightly across one of the high-speed streaks. Thus one is seeing high shear in the experiments that is lying slightly off-peak in the simulations. The spanwise spacing of the first streaks, measured in wall units of the fully developed flow, is between 80 and 150, depending on streamwise position and time. This is comparable to the value of 120 found by Nishioka *et al.*, and the average turbulent value of about 100. This characteristic length seems to be set from very early on in the transition process, since the spacing of the streaks is fixed by the spacing of the streamwise vortices which evolve from the first shear-layer roll-up.

A wave-like instability develops in the detached secondary shear layer. In the pressure contours at $t = 151$ and 153 (figure 12) one can observe along the length of the shear layer the appearance of alternatively positive and negative p'. The low-pressure regions correspond to the cores of newly developing vortices, while the high-pressure regions are the stagnation-point regions between successive vortices. The roll-up of these new vortices breaks up this shear layer by $t = 153$. The location of the vortices along the shear layer indicates that once again we have a shear-layer mechanism for strengthening the vortices. The original disturbances are the large irregularities along the shear-layer length, from the preceding events in the flow. The application of shear then causes roll-up into discrete vortices.

The shear-layer roll-up process described in the preceding paragraph has many similarities with the development of an artificial low-speed streak, investigated experimentally by Acarlar & Smith (1987). They were interested in the problem as a model of the near-wall region of the turbulent boundary layer. The low-speed

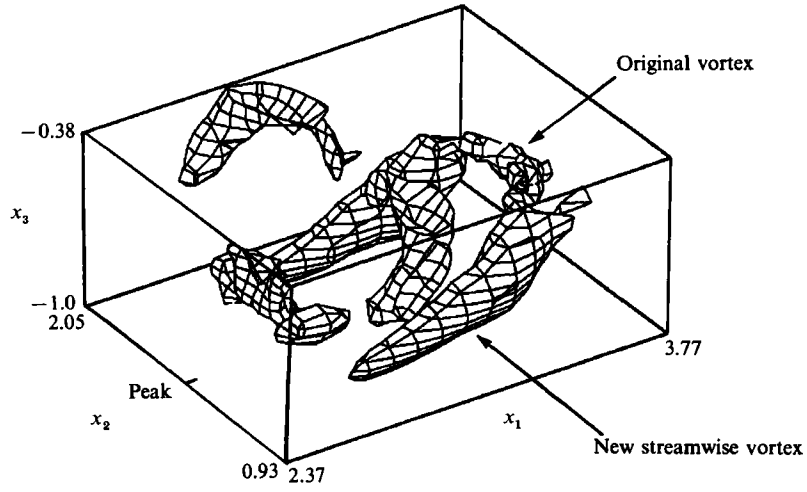

FIGURE 15. View of one of the vortical structures that developed from roll-up of the second-generation shear layer. The pressure surface $p' = -0.02$ is shown at $t = 156$ in a small subsection of the computational domain.

streak was generated by blowing in a streamwise slot. This generated an inflexional shear layer away from the wall, which rolled up into vortices. These then evolved into a hairpin shape. A similar process was observed in the simulation, although clear hairpin vortices were not observed. In particular, one of the vortices developing out of the second-generation shear layer was followed as it evolved in time. This vortex can be seen at $t = 155$ in the shear and pressure contours at $x_1 = 3.2$ on figure 12. This vortex forms initially with a barrel shape at $t = 153$. Figure 15 shows a view of this region of the flow at the slightly later time $t = 156$. Only a reduced domain is shown, since we are here looking for small-scale features in an increasingly complicated flow. Strong streamwise vortices have formed in the near-wall region. These vortices are connected to each other by a thin strand of low pressure, which is all that remains of the original vortex. It is not clear whether this vortex has evolved into the streamwise vortices, or whether is has simply acted as the trigger to convert the vertical vorticity at the edges of the high-speed streak into streamwise vorticity. In either case the final result is a strong streamwise vortex in the near-wall region. The final structure does not have a clear hairpin shape, but it does appear that the mechanism at work is very similar to that described by Acarlar & Smith. Similar to turbulent flow (Kline 1990) the vortices that are observed are of much shorter streamwise length than the low-speed streaks.

By time $t = 155$ in the simulation it appears that a cyclical process has been established that is capable of repeating itself indefinitely. This process is sketched on figure 16. Streamwise vortices near the wall generate detached shear layers as well as regions of high wall shear. The former roll up into new vortices, which either evolve in three dimensions into new streamwise vortices or serve to kick the vertical vorticity at the interface between the low-speed and high-speed streaks into streamwise vorticity. The cycle continues when the new streamwise vortices generate new shear layers. This process contains many of the characteristics of near-wall turbulence. It includes a mechanism for the generation of regions of high wall shear, with low-speed streaks in between. The individual roll-up events in the shear layer generate fluid motions away from the wall (ejections) and motions towards the wall (sweeps). The wave-like form of the shear-layer roll-up is a possible explanation of a

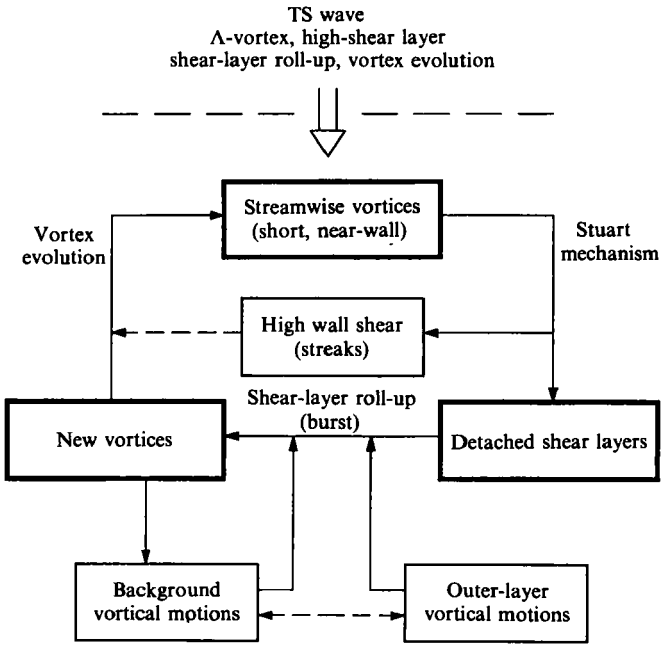

FIGURE 16. Schematic of the cyclical process of near-wall turbulence, as it appears in the late stages of the transition process.

burst (a high-activity process, incorporating a number of ejections and sweeps). A difference between this elementary turbulence and recent ideas on fully developed turbulence (Robinson 1991; Jimenez & Moin 1991) lies in the symmetry of the current process. The first turbulence forms near the peak plane, which is a plane of symmetry in the simulation (as in transition experiments with forced TS waves). Thus the vortical structures that form are also symmetric. However, such symmetric structures are rarely observed in simulations of fully developed turbulence, where single quasi-streamwise vortices are the rule. In this connection we can make two comments. First, it appears that the imposed symmetry is not a barrier to the formation of a turbulent flow. Indeed, turbulence statistics from the current simulation (Gilbert 1988) are almost identical to the statistics for Kim *et al* (1987), who did not assume any symmetries. Secondly, it would be useful to know whether the shear-layer development and roll-up is an important a part of the asymmetric mechanisms of turbulence as of the symmetric case.

5. Predictability

A characteristic of turbulent flow is its unpredictability, in the sense that two turbulent flows which are initially very close to the each other will diverge over time and eventually become completely decorrelated. In this section the issue of unpredictability in the transitional channel flow is investigated, but treated separately from the development of the mechanics of turbulent flow (see §4).

The symmetry in the initial condition between the upper and lower channel halves can be exploited to reveal the nature of the growth of unpredictability. This symmetry was not incorporated into the numerical method (unlike the spanwise symmetry) and was therefore free to disappear due to the unpredictability effect, triggered by differences in the initial condition or by roundoff error. The accuracy of

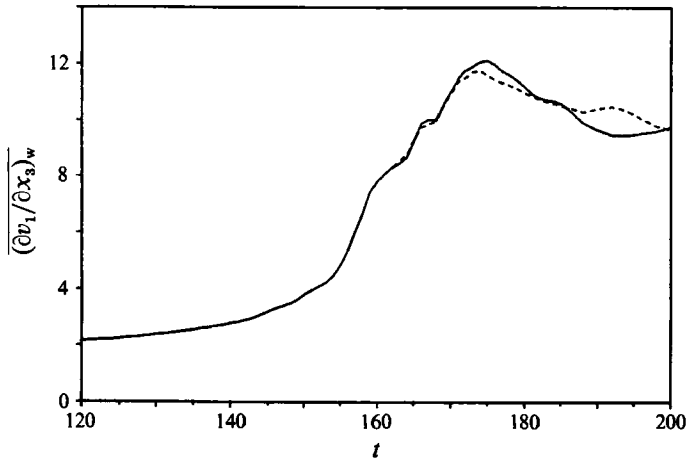

FIGURE 17. Mean wall shear measured on the upper (——) and lower (– – – –) channel walls, showing the loss of symmetry at later times in the simulation.

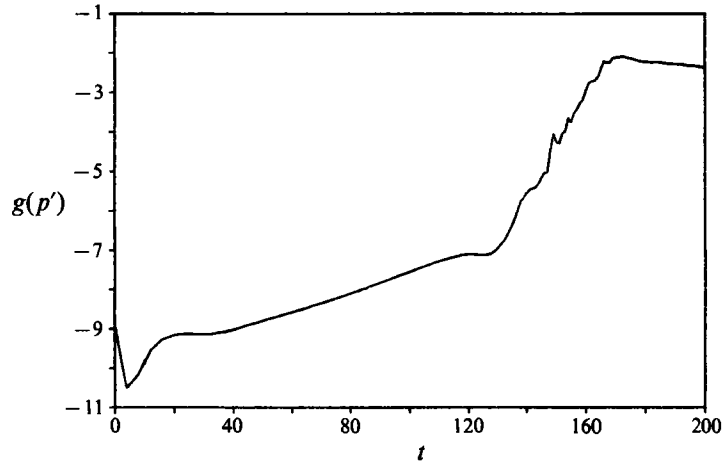

FIGURE 18. The asymmetry measure $g(p')$, showing the loss of predictability during the transition process. Note the sharp change of slope at $t = 130$.

the symmetry in the initial condition was found to be 5 decimal places in the pressure, probably fixed by the method of including the linear stability eigenfunctions. An example of the loss of symmetry is shown by the mean wall shear, plotted on figure 17 for both the upper and lower wall during the simulation. It can be seen that initially the curves lie on top of each other, due to the initial symmetry. However, from around $t = 165$ onwards the two walls have shear levels that are visibly different from each other. At certain spanwise positions the differences were found to be rather large. The question to be addressed is where this loss of predictability comes from.

A quantitative measure of the asymmetry can be defined by a functional g, given by

$$g(f) = \log_{10}\left\{\frac{1}{N}\Sigma(f_l - f_u)^2\right\}^{\frac{1}{2}} \tag{2}$$

where f_l and f_u are the values of a function f in the lower and upper channel halves at points where $f_l = f_u$ with perfect symmetry, and the summation is over $N = N_1 \times N_2 \times \frac{1}{2}N_3$ points. This quantity is analogous to the largest Lyapunov

exponent of the flow. It is different in that the two channel halves are not strictly independent of each other, and the level of the asymmetry is not maintained infinitesimally small. A plot of $g(p')$ is shown on figure 18. Several distinct regions are apparent. For $t < 120$ a nearly linear growth in g is obtained (ignoring the initial transient, $t \leqslant 40$). Expressing the growth of the asymmetry as $e^{\sigma t}$, we have $\sigma = 0.05$ in this region. At these times the flow is governed by the growth of the secondary instability, and it is clear that if the two channel halves have slightly different initial conditions the difference will grow at the secondary instability growth rate. This growth rate was found by Herbert (1983) to be $\sigma = 0.0484$, which compares well with the growth rate of the asymmetry. Around $t = 130$ there is a dramatic change. The value of σ increases sixfold to $\sigma \approx 0.32$, which lasts until the two channel halves become decorrelated and the value of g reaches a plateau ($t > 170$).

The increased value of σ in the late stages of the transition process is very interesting and may be due to several physical effects. One is the appearance of strong shear layers for these later times, which will amplify any differences between the two channel halves very strongly, owing to the high growth rate of the inflexional instability. Another physical phenomenon is the appearance of discrete vortices for these later times in the transition process. As vortices move and interact with each other, small differences in the initial position will be amplified and will lead to a loss of predictability. It is remarkable that, in spite of the multitude of physical phenomena at work and the large spanwise variations, the growth of unpredictability continues at the same rate ($\sigma = 0.32$) over the large time span $t = 140$ to 170. For comparison, we can quote values for σ from Métais & Lesieur (1986), who studied unpredictability in two-dimensional turbulence using EDQNM theory. They obtained $\sigma = 0.26$ for unforced isotropic turbulence, and $\sigma = 0.38$ for the forced case.

The time of $t = 170$ for decorrelation becomes larger if the initial symmetry is accurate to more decimal places. To test this another simulation was run in which the symmetry in the initial condition was imposed to machine accuracy (64 bits). The result was that the appearance of the plateau corresponding to decorrelation was delayed to $t \approx 210$. What is notable is that the loss of predictability occurs very late in the transition process. Up to this point the details of the flow are determined entirely by the initial condition of the simulation. In particular it should be pointed out that the roll-up of the shear layer into discrete vortices occurs while the asymmetry is still insignificantly small, and that therefore the vortex roll-up process is deterministic, and not triggered by the growth of random background noise. This is in agreement with the findings of Borodulin & Kachanov (1989), but contradicts the conventional tertiary instability concept from for example Nishioka *et al.* (1980).

6. Large-scale structures and spanwise evolution

The method of locating vortical structure by low-pressure regions was applied to 35 data fields in the late stages of transition, from $t = 138$ to 172. Three large-scale structures (excluding the original Λ-vortex) were found to develop and then break up. Three views of the first of these structures, the hairpin vortex, are shown on figure 19 (*a*) for the pressure surface $p' = -0.025$. The origin and development of this structure have been described in §3. The details in the pressure surface can be traced to the interactions between the various levels of roll-up of the shear layer that formed around the Λ-vortex from the secondary instability of the flow. The hairpin structure breaks up at $t = 148$.

A new structure appears in the flow from $t = 153$ to 157, shown at $t = 156$ on figure

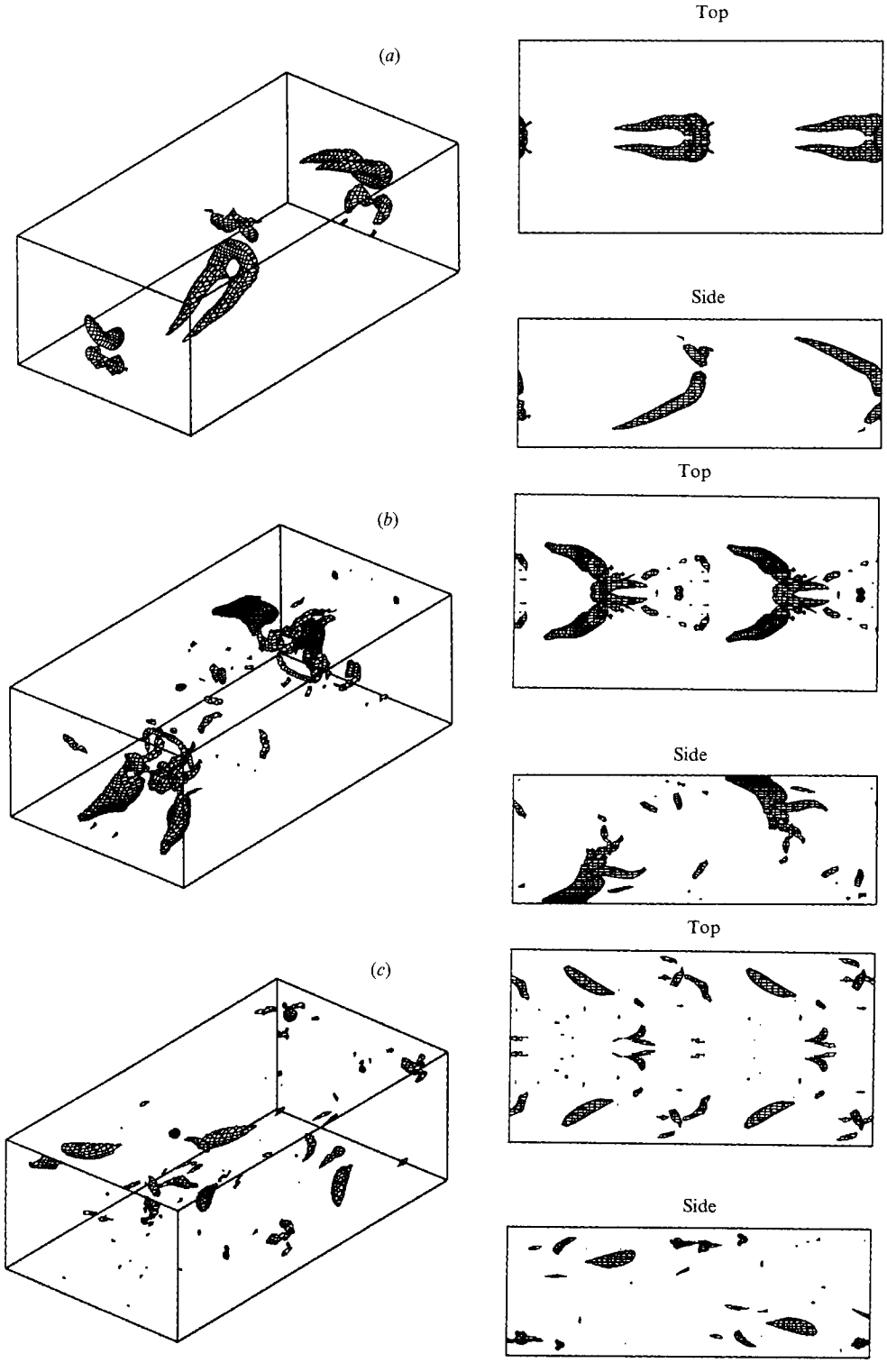

FIGURE 19. Large-scale structures: (*a*) hairpin vortex at $t = 145$ ($p' = -0.025$), (*b*) vortex at $t = 156$ ($p' = -0.035$) and (*c*) late inverted Λ-vortex at $t = 162$ ($p' = -0.035$).

19(*b*) for the pressure surface $p' = -0.035$. The strongest regions of rotation (lowest pressure) are the trailing legs at $x_1 = \frac{1}{8}L_1$, about halfway between the peak and valley planes. Very near to the wall these legs are oriented in the streamwise direction. The nearness to the wall means that this structure leaves a very strong 'footprint' in terms of wall pressure. The origin of this structure is not clear, but parts of it trace back to the third level of roll-up of the original shear layer. This structure evolves rapidly in time and breaks up at about $t = 157$.

A third and final large-scale structure appears briefly at $t = 162$ near the valley location. This is shown on figure 19(*c*) for $p' = -0.035$, and appears as a Λ-shaped vortex, though with the point of the Λ facing upstream, which is opposite to the Λ-vortex that developed from the secondary instability. It is located at around $x_1 = \frac{3}{4}L_1$ in the lower channel half, and at around $x_1 = \frac{1}{4}L_1$ in the upper channel half. This structure exists very late in the transition process – at the same time that the features of developed wall turbulence have appeared in the peak region. The origin of this structure, and its relation to the high-shear layer at the valley (observed by Gilbert 1988), needs further investigation.

At the same time that these large-scale structures are forming and breaking up, the region in which the near-wall flow contains the features of wall turbulence is extending in the spanwise direction. The wall shear is shown on figure 20 for levels of 0 (dashed), 10 and 20 at $t = 162$, 172 and 182. At $t = 162$ the region around the peak plane shows the streaky structure that is characteristic of the turbulent sublayer. The interior of the channel calms down at the later times and the streaky structure spreads across the whole of the channel width.

The existence of strong spanwise variations in the transition process is well known (more details can be found in Gilbert 1988), and can be clearly seen in the instantaneous views of the transition process. These variations would be obscured by conventional averaging across the whole flow domain. Instead, we divide the region between the peak and valley into four equally spaced strips and present averages in these strips. Region 1 denotes the strip next to the valley plane and region 4 the strip next to the peak plane. The strong dependence of wall shear on spanwise position is shown on figure 21(*a*). The time history shows that high wall shear first develops in region 4 (peak), and that by $t = 162$ high wall shear is found in both regions 3 and 4, while the wall shear in region 1 is still near its laminar value. This development of high wall shear in region 1 (valley) is retarded relative to regions 3 and 4 by 10–15 time units. The wall shear in all regions shows an overshoot relative to the turbulent time-averaged value of 9.4. The mean centreline velocity also shows a strong dependence on spanwise position. Figure 21(*b*) shows how the mean centreline velocity departs from the laminar value in region 4 (peak) at $t = 143$, but remains close to the laminar value in region 2 up to $t = 163$. Similar spanwise dependence was observed in the mean velocity profiles and in plots of the maximum and minimum pressure during the simulation. Figure 22 shows mean velocity profiles in each region at various times during the simulation. It can be seen that in region 4 the mean velocity profile has a recognizably turbulent form by $t = 162$, while in region 1 a turbulent profile is not obtained until $t = 178$.

7. Discussion

7.1. *Generality of findings*

To check the generality of the observations made in the preceding sections for K-type transition, a similar investigation has been made for both H-type (subharmonic) and

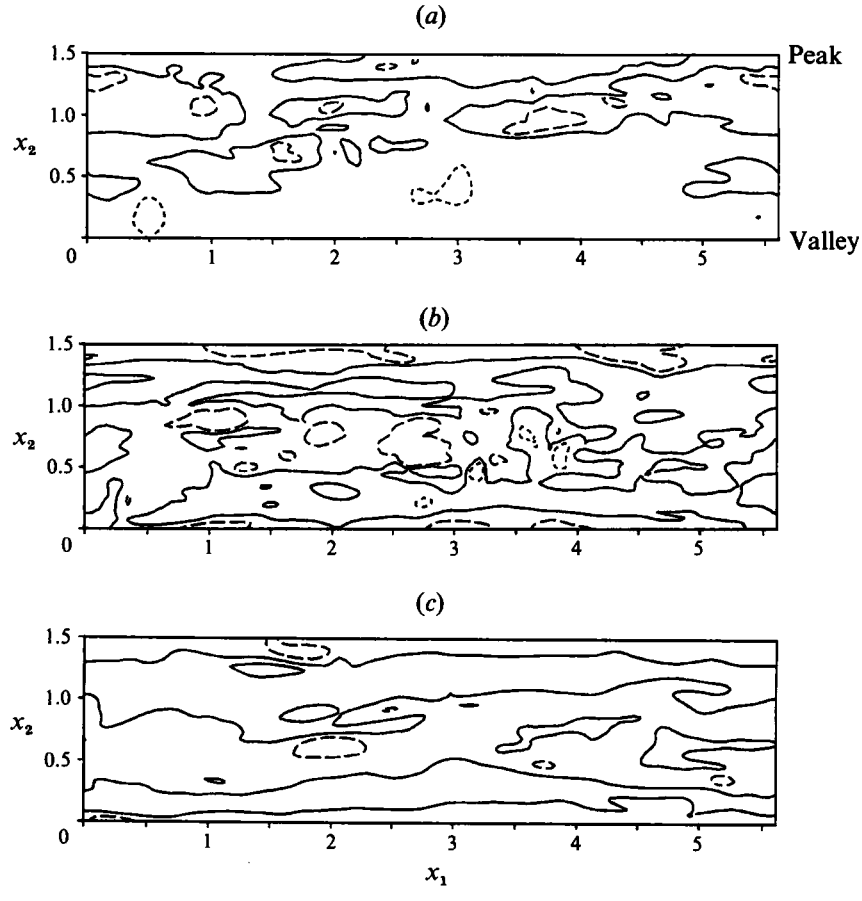

FIGURE 20. Wall shear at (*a*) $t = 162$, (*b*) 172 and (*c*) 182, showing the spreading of the streaky sublayer structure in the spanwise direction. Contours are shown of $\partial v_1/\partial x_3 = 0$ (- - - -), 10 (——) and 20 (– – – –).

mixed-type transition. The initial conditions for these simulations were described in §2.1.

The H-type transition is interesting because the lower half of the channel undergoes transition before the upper half, and thus cross-channel interactions are avoided. This case may therefore have more features in common with boundary-layer transition. A summary of the observed process is shown in the vortex trajectory plot on figure 23. Vortices L1, L1a, L2, L2a, L3 and L3a were observed. Vortex L1 developed into a headless hairpin vortex (only the legs showed up as strong pressure minima). Vortex L1a had no clearly identifiable shape, while vortices L2, L2a and L3 all began life with a banana shape, evolving into what might be loosely termed hairpin vortices, but without the long legs of a 'true' hairpin vortex (such as in figure 19*a*).

The mixed-type transition was the most complex, although definite shear-layer roll-up could be observed, producing vortices L1, L1a, L2, L2a and L3 in the lower channel half and vortices U1, U2, U2a and U3 in the upper channel half. These are shown on a trajectory plot on figure 24. Almost immediately after formation there was a strong cross-channel interaction between vortices L2 and U1, leaving a

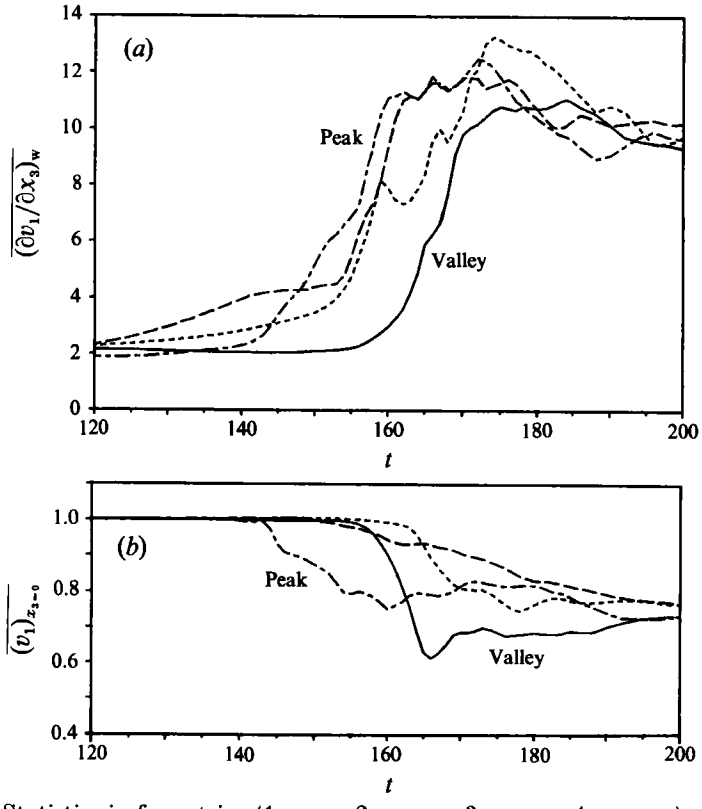

FIGURE 21. Statistics in four strips (1, ——; 2, - - - - -; 3, — — —; 4, — - —): (*a*) wall shear (average turbulent value 9.4) and (*b*) centreline streamwise velocity (average turbulent value 0.755).

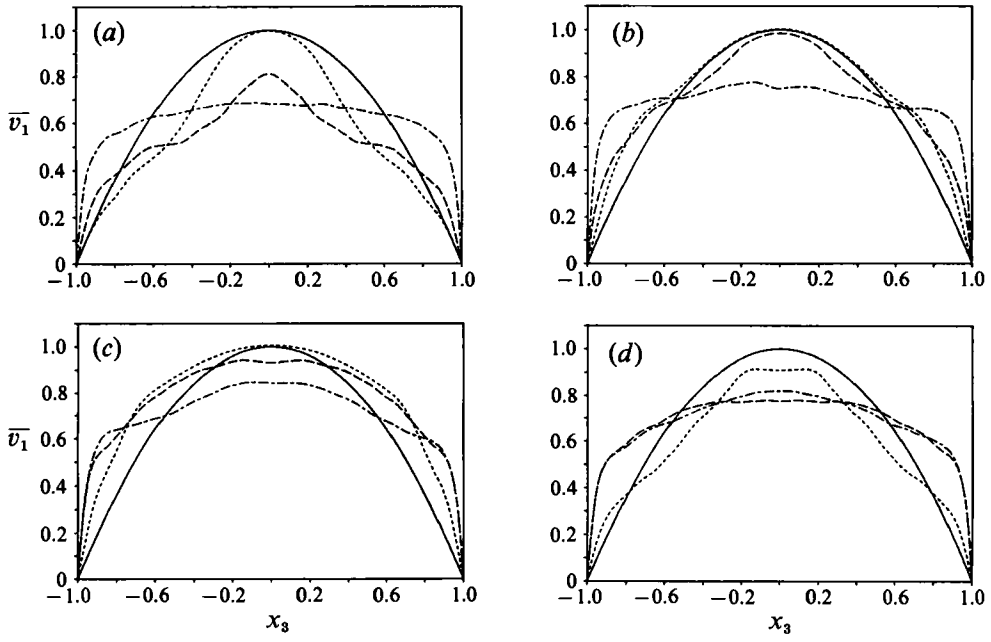

FIGURE 22. Mean velocity profiles, averaged in four strips: (*a*) region 1 = valley, (*b*) region 2, (*c*) region 3, (*d*) region 4 = peak, at times 0 (——), 146 (- - - - -), 162 (— — —) and 178 (— - —).

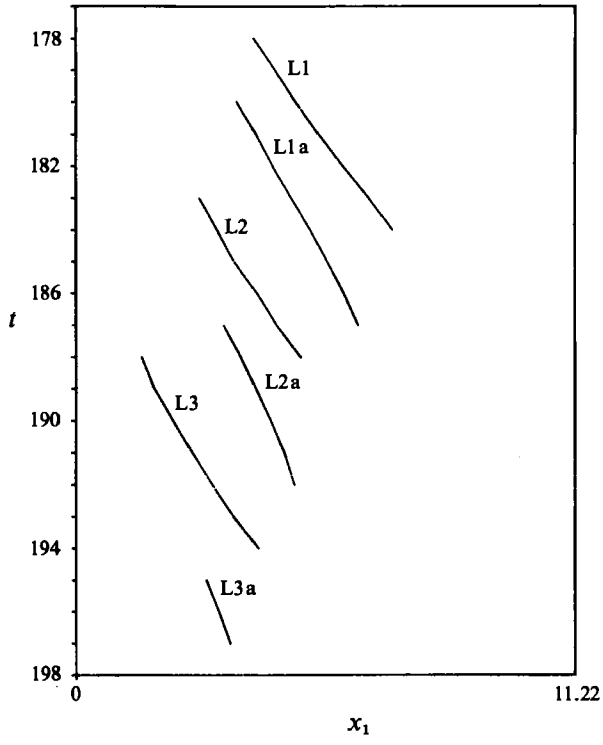

FIGURE 23. Trajectories of the vortices forming from the high-shear-layer roll-up from a simulation of subharmonic transition.

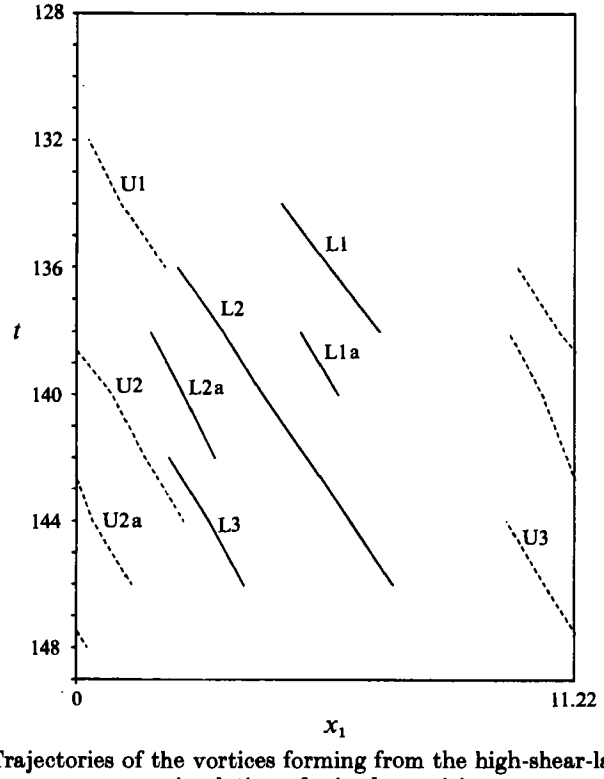

FIGURE 24. Trajectories of the vortices forming from the high-shear-layer roll-up from a simulation of mixed transition.

complex three-dimensional vortex behind. Only one of the vortices (U2) turned into a recognizable hairpin vortex.

Although the detailed interactions between the vortices were very different between the three simulations studied, important elements remained the same. The original shear-layer roll-up followed the general behaviour sketched on figure 8, with vortices forming in pairs, separated by about $\frac{3}{4}$ of a TS wave. It is interesting to note that the shedding frequency did not change for these new cases. Also, from the staggered arrangement of the Λ-vortices in subharmonic transition it is clear that the later roll-up of vortices in the shear layer is not caused by the overlapping of vortices from earlier roll-up processes. In the subharmonic case the box length is large enough so that there are none of these overtaking interactions. Thus the roll-up mechanism appears to be inherent to the Λ-vortex and not influenced by outside events in the flow.

In each simulation second-generation shear layers were again observed which developed a new instability (the details were again different – the shear layer was inclined at 30° for the H-type simulation, as compared to near-horizontanl for the K-type simulation). In the case of H-type transition the staggered symmetry was exploited to check the issue of loss of predictability, with similar results to K-type transition.

7.2. *Interpretation of 'breakdown'*

Until about 10 years ago the common explanation for the formation of spikes in the velocity–time traces was that a high-frequency instability took place in the high-shear layer, amplifying background disturbances in the flow. Thus, beyond the primary and secondary instabilities there was still a need to invoke a stochastic input in order to get transition to turbulence. This picture was doubted by Kleiser (1982, 1985), on the basis that the high-frequency components of the energy spectrum grew continuously from the secondary instability stage, long before the appearance of the high-shear layer. Kachanov *et al.* (1985) claimed that the development of the spikes is an entirely deterministic event, and is not involved in the development of unpredictability (Kachanov calls this 'randomization') in the flow. This viewpoint is entirely supported by the observation in § 5 of this paper that the shear-layer roll-up occurs in exactly the same way in both halves of the channel, well before the two halves become decorrelated. This is not to say that the instability of the shear layer is not important, and we do not doubt the results of the instability calculations based on instantaneous velocity profiles made by Nishioka *et al.* (1980). This kind of instability is one route to the loss of predictability of the flow. It may even, in applications with high background noise, lead to premature roll-up of the high-shear layer. However, it is important to note that the extra background noise is not a necessary condition for the generation of turbulence. Turbulence can develop in a quite deterministic fashion from the secondary instability stage onwards.

Elements from the tertiary instability concept do seem to be correct. The vortices do develop in the shear layer, and the mechanism for their growth is the same as the mechanism for growth of vortices in a shear layer triggered by an inflexional instability. The question is in the origin of the disturbance that triggers the growth: random background noise, or a deterministic kick. In this respect, we can draw an analogy to the vortices that form when a free shear layer, such as a mixing layer, is started. A start-up vortex pair is observed that grows and moves downstream, followed by the growth of a Kelvin–Helmholtz instability in the newly established shear layer. The process, including the generation of a pair of vortices, can be observed in a simulation by Grinstein, Oran & Boris (1985). (The resolution of this

simulation might appear borderline, but based on some earlier work by the first author on spatially developing mixing layers it is believed that the start-up phenomenon has been correctly captured.) That we have two kinds of shear-layer phenomena is apparent if we ask the question: what happens as the background noise approaches zero? In this case the Kelvin–Helmholtz instability has nothing to amplify and no vortices form. However, the start-up vortices remain. We believe that the spikes are the result of vortices that form deterministically, similar to the start-up vortices in a mixing layer.

A theoretical description of the shear-layer vortex formation and evolution does not at present exist. The structure of the shear-layer evolution (as pairs of vortices separated by a fairly large distance, figure 8) suggests that a solitary-wave approach might be useful. In this case the pairs of vortices could form by splitting of a solitary wave. A separate mechanism would then have to be invoked to explain the nonlinear kick that serves to start the growth of each wave. The idea that the spikes might be treated as solitary waves has been pursued recently by the Novosibirsk group (Borodulin & Kachanov 1989; Kachanov 1990). Their work has mainly been to demonstrate certain similarities between the spikes and solitary waves. A useful theory of breakdown incorporating solitary waves seems distant.

8. Conclusions

By studying data from a direct numerical simulation of the complete transition process in plane channel flow, we have obtained a fairly complete picture of the formation, evolution and breakup of vortices in the late stages of transition, from the Λ-vortex stage (resulting from the secondary instability of finite-amplitude Tollmien–Schlichting waves) up to fully developed turbulence. Important results are the following.

(i) A detailed investigation of the vortices that form in the high-shear layer around the Λ-vortices reveals that each roll-up generates a pair of vortices, although the second vortex in each pair is usually weak. Three levels of roll-up were observed, with a total of five significant vortices in each channel half. The vortices form as a result of a deterministic vortex-shedding process, rather than being triggered by the growth of random background disturbances.

(ii) Only one of the vortices (from each set of five) is found to develop into a strong hairpin-shaped structure. Results from other simulations confirm that hairpin vortices are the exception, rather than the rule, for the vortices that develop from the high-shear layer around each Λ-vortex. The simplified statement, often found in the literature, that the high-shear layer rolls up into hairpin vortices, is therefore a little misleading.

(iii) In the subsequent evolution it is found that interactions between vortices from opposite channel halves (cross-channel interactions), and between vortices in the same channel half (overtaking interactions), are important. Due to one of these interactions the hairpin vortex does not develop into a vortex ring.

(iv) A cyclic sequence of phenomena is observed near the peak plane, which has all the important characteristics of near-wall turbulence. The starting point for this sequence is the presence of quasi-streamwise vortices in the near-wall region. These arise from the evolution of the vortices that form in the high-shear layer around the Λ-vortices. These quasi-streamwise vortices generate high wall shear and detached second-generation shear layers, which subsequently roll up into new vortices. The remainder of the transition process consists of the spreading of this mechanism to

other spanwise positions. Large-scale vortical motions play an important part in this process.

This work was carried out while the first author was a Guest Scientist at DLR, and was partly supported by the Deutsche Forschungsgemeinshaft. The authors would like to thank N. Gilbert, who generated the databases used in the study and supplied the initial post-processing software. H. Vollmers provided the graphics software for the three-dimensional plots. A preliminary version of this paper was presented at the Royal Aeronautical Society Conference on Boundary-Layer Transition and Control in Cambridge, UK, April 8-11, 1991.

REFERENCES

ACARLAR, M. S. & SMITH, C. R. 1987 A study of hairpin vortices in a laminar boundary layer. Part 2. Hairpin vortices generated by fluid injection. *J. Fluid Mech.* **175**, 43–83.

BORODULIN, V. I. & KACHANOV, Y. S. 1989 Role of the local secondary instability mechanism in the K-mode breakdown of the boundary layer. *Sov. J. Appl. Phys.* **3**, 70–81.

CANUTO, C., HUSSAINI, M. Y., QUARTERONI, A. & ZANG, T. A. 1988 *Spectral Methods in Fluid Dynamics*. Springer.

CHONG, M. S., PERRY, A. E. & CANTWELL, B. J. 1990 A general classification of three-dimensional flow fields. *Phys. Fluids* A**2**, 765–777.

GILBERT, N. 1988 Numerische Simulation der Transition von der laminaren in die turbulente Kanalströmung. Dissertation, University of Karlsruhe. *Rep. DFVLR-FB* 88–55. (ESA English translation, to appear.)

GILBERT, N. & KLEISER, L. 1990 Near-wall phenomena in transition to turbulence. In *Near-Wall Turbulence* (ed. S. J. Kline & N. H. Afgan), pp. 7–27. Hemisphere.

GRINSTEIN, F. F., ORAN, E. S. & BORIS, J. P. 1986 Numerical simulations of axisymmetric mixing in planar shear flows. *J. Fluid Mech.* **165**, 201–220.

HAMA, F. R. & NUTANT, J. 1963 Detailed flow-field observations in the transition process in a thick boundary layer. In *Proc. 1963 Heat Transfer and Fluid Mech. Inst.*, pp. 77–93.

HÄRTEL, C. & KLEISER, L. 1992 Subharmonic transition to turbulence in channel flow. *Fourth European Turbulence Conf., Delft, The Netherlands, June 30–July 3, 1992.*

HERBERT, TH. 1983 Stability of plane Poiseuille flow – theory and experiment. *Fluid Dyn. Trans.* **11**, 77–126.

HERBERT, TH. 1988 Secondary instability of boundary layers. *Ann. Rev. Fluid Mech.* **20**, 487–526.

HUNT, J. C. R., WRAY, A. A. & MOIN, P. 1988 Eddies, streams and convergence zones in turbulent flows. In *Proc. 1988 Summer Program, NASA-Stanford Center for Turbulence Research*, pp. 193–208.

JIMENEZ, J. & MOIN, P. 1991 The minimal flow unit in near-wall turbulence. *J. Fluid Mech.* **225**, 213–240.

KACHANOV, YU. S. 1990 Secondary and cascade resonant instabilities of boundary layers. Wave-resonant concept of a breakdown and its substantiation. In *Laminar-Turbulent Transition* (ed. D. Arnal & R. Michel), pp. 65–80 Springer.

KACHANOV, YU. S., KOZLOV, V. V., LEVCHENKO, V. YA. & RAMAZANOV, M. P. 1985 On nature of K-breakdown of a laminar boundary layer. New experimental data. In *Laminar-Turbulent Transition* (ed. V. V. Kozlov), pp. 61–72. Springer.

KIM, J., MOIN, P. & MOSER, R. 1987 Turbulence statistics in fully developed channel flow at low Reynolds number. *J. Fluid Mech.* **177**, 133–166.

KLEBANOFF, P. S., TIDSTROM, K. D. & SARGENT, L. M. 1962 The three-dimensional nature of boundary-layer instability. *J. Fluid Mech.* **12**, 1–34.

KLEISER, L. 1982 Numerische Simulationen zum laminar-turbulenten Umschlagsprozeß der ebenen Poiseuille-Strömung. Dissertation, University of Karlsruhe; *Rep.* KfK 3271, Kernforschungszentrum Karlsruhe.

KLEISER, L. 1985 Three-dimensional processes in laminar–turbulent transition. In *Nonlinear*

Dynamics of Transcritical Flows (ed. H. L. Jordan, H. Oertel & K. Robert). Lecture Notes in Engineering, vol. 13, pp. 123–154. Springer.

KLEISER, L. & LAURIEN, E. 1985 Three-dimensional numerical simulation of laminar-turbulent transition and its control by periodic disturbances. In *Laminar-Turbulent Transition*, (ed. V. V. Kozlov), pp. 29–37. Springer.

KLEISER, L. & SCHUMANN, U. 1980 Treatment of incompressibility and boundary conditions in 3-D numerical spectral simulations of plane channel flows. In *Proc. 3rd GAMM Conf. on Numerical Methods in Fluid Mechanics* (ed. E. H. Hirschel), pp. 165–173. Vieweg.

KLEISER, L. & ZANG, T. A. 1991 Numerical simulation of transition in wall-bounded shear flows. *Ann. Rev. Fluid Mech.* **23**, 495–537.

KLINE, S. J. 1990 Comment in *Whither Turbulence? Turbulence at the Crossroads* (ed. J. Lumley), Lecture Notes in Physics, vol. **357**, pp. 383–388. Springer.

KLINE, S. J., REYNOLDS, W. C., SCHRAUB, F. A. & RUNSTADLER, P. W. 1967 The structure of the turbulent boundary layer. *J. Fluid Mech.* **30**, 741–773.

KOVASZNAY, L. S. G., KOMODA, H. & VASUDEVA, B. R. 1962 Detailed flow field in transition. In *Proc. 1962 Heat Transfer and Fluid Mech. Inst.*, pp. 1–26.

MÉTAIS, O. & LESIEUR, M. 1986 Statistical predictability of decaying turbulence. *J. Atmos. Sci.* **43**, 857–870.

MOIN, P., LEONARD, A. & KIM, J. 1986 Evolution of a curved vortex filament into a vortex ring. *Phys. Fluids* **29**, 955–963.

NISHINO, K. & KASAGI, N. 1989 Turbulence statistics measurement in a two-dimensional channel flow using a three-dimensional particle tracking velocimeter. In *Seventh Symp. on Turbulent Shear Flows, Stanford University, Stanford, CA, Paper* 22–1.

NISHIOKA, M. 1985 Laminar-turbulent transition in plane Poiseuille flow. In *Recent Studies on Turbulent Phenomena* (ed. T. Tatsumi, H. Maruo & H. Takami), pp. 193–203. Tokyo: Association for Science Documents Information.

NISHIOKA, M. & ASAI, M. 1984 Evolution of Tollmien-Schlichting waves into wall turbulence. In *Turbulence and Chaotic Phenomena in Fluids* (ed. T. Tatsumi), pp. 87–92.

NISHIOKA, M., ASAI, M. & IIDA, S. 1980 An experimental investigation of the secondary instability. In *Laminar-Turbulent Transition* (ed. R. E. Eppler & H. Fasel), pp. 37–46. Springer.

NISHIOKA, M., ASAI, M. & IIDA, S. 1981 Wall phenomena in the final stage of transition to turbulence. In *Transition and Turbulence* (ed. R. E. Meyer), pp. 113–126. Academic.

NISHIOKA, M., IIDA, S. & ICHIKAWA, Y. 1975 An experimental investigation of the stability of plane Poiseuille flow. *J. Fluid Mech.* **72**, 731–751.

PERRY, A. & CHONG, M. S. 1987 A description of eddying motions and flow patterns using critical-point concepts. *Ann. Rev. Fluid Mech.* **19**, 125–155.

RIST, U. 1990 Numerische Untersuchung der räumlichen, dreidimensionalen Störungsentwicklung beim Grenzschichtumschlag. Dissertation, University of Stuttgart.

ROBINSON, S. K. 1991 Coherent motions in the turbulent boundary layer. *Ann. Rev. Fluid Mech.* **23**, 601–639.

SANDHAM, N. D. & REYNOLDS, W. C. 1991 Three-dimensional simulations of large eddies in the compressible mixing layer. *J. Fluid Mech.* **244**, 133–157.

STUART, J. T. 1965 The production of intense shear layers by vortex stretching and convection. *AGARD Rep.* 514.

STUART, J. T. 1984 Instability of laminar flows, nonlinear growth of fluctuations and transition to turbulence. In *Turbulence and Chaotic Phenomena in Fluids* (ed. T. Tatsumi), pp. 17–26. Elsevier.

VOLLMERS, H., KREPLIN, H.-P. & MEIER, H. U. 1983 Separation and vortical-type flow around a prolate spheroid – evaluation of relevant parameters. *AGARD Conf. Proc.* 342, Paper 14.

WILLIAMS, D. R., FASEL, H. & HAMA, F. R. 1984 Experimental determination of the three-dimensional vorticity field in the boundary-layer transition process. *J. Fluid Mech.* **149**, 179–203.

ZANG, T. A. & KRIST, S. E. 1989 Numerical experiments on stability and transition in plane channel flow. *Theor. Comput. Fluid Dyn.* **1**, 41–64.